

Infrared 7.6- μm lead-salt diode laser heterodyne radiometry of water vapor in a CH_4 -air premixed flat flame

Damien Weidmann and Daniel Courtois

We deal with the design of a diode laser heterodyne radiometer and its application in a combustion process. We present some experimental results obtained with a CH_4 -air premixed flat flame as the optical source. The goal is to prove that heterodyne detection techniques are relevant in remote detection and diagnostics of combustion and can have important applications in both civil and military fields. To the best of our knowledge, it is the first time that this demonstration is made. The radiometer, in spite of the low-power lead-salt diode laser used as a local oscillator, enables us to record high-temperature water-vapor emission spectra in the region of 1315 cm^{-1} . © 2003 Optical Society of America

OCIS codes: 300.2140, 300.6310, 300.6320, 300.6340, 280.2470, 280.3420.

1. Introduction

Laser heterodyne radiometry offers the great advantage of being a completely passive technique to achieve remote sensing. This feature provides discretion, which is particularly attractive for military and surveillance applications. In addition, in contrast to an active way of sensing in which a probe laser beam is needed, a totally passive technique allows long-range monitoring.

This technique is particularly attractive in the middle-infrared region of the electromagnetic spectrum, which corresponds to the emission or absorption spectra of several atmospheric molecules. It offers both high spatial and spectral resolutions and great sensitivity.

The laser heterodyne radiometer can be used mainly in two ways. In the first one, the Sun (or any other distant radiative source) is used as a blackbody source whose radiation goes through the Earth's atmosphere. In this case, the radiometer resolves ab-

sorption spectra of atmospheric molecules. In the second one, the source of radiation is the emission of molecular gas, which can be detected if a thermal contrast with the background exists. In this case, the radiometer resolves the emission spectra of the radiating molecular species.

These two techniques were originally developed with a CO_2 laser as the local oscillator. Several authors reported concentration measurements of atmospheric constituents.¹⁻⁶ The characterization of weak molecular emission lines was mainly used in the field of astronomy, to detect emission lines from extraterrestrial atmospheres.⁷⁻⁹ But use of a gas laser as a local oscillator is restrictive on the frequency tunability. For this reason, semiconductor lasers are preferred to gas lasers.

Semiconductor lasers allow a wide frequency tunability; any region of the optical spectrum can be theoretically reached. But they are far from an ideal laser: The emitted beam is astigmatic and elliptic, and the single-mode optical power available is low.^{10,11} In any case, the advantage of continuous frequency tunability is prevalent. A number of authors have reported some heterodyne experiments with semiconductor lasers: Frerking and Muehlner were the pioneers,¹² and several other researchers probed the Earth's atmosphere¹³⁻¹⁶ or interstellar objects.¹⁷

In this paper we apply the infrared heterodyne detection technique to characterize the thermal emission of a high-temperature molecular species pro-

The authors are with Groupe de Spectrométrie Moléculaire et Atmosphérique, Unité Mixte de Recherche, Centre National de la Recherche Scientifique 6089, Université de Reims Champagne-Ardenne, Unité de Formation et de Recherche Sciences Exactes et Naturelles, B.P. 1039, 51687 Reims Cedex 2, France. The e-mail address of D. Weidmann is damien.weidmann@univ-reims.fr.

Received 19 March 2002; revised manuscript received 4 November 2002.

0003-6935/03/061115-07\$15.00/0

© 2003 Optical Society of America

duced by a combustion reaction. This technique has the advantage of being able to perform passive remote-sensing experiments in the burned gas region of combustion reactions. For example, this technique can be applied to characterize pollutants generated by aircraft thrust nozzles or industrial burners. Molecules such as NO, NO₂, CO, and SO₂ can be detected in the middle-infrared region.

In this paper we report the conception of the heterodyne radiometer dedicated to observe emission lines in the postflame region of a CH₄-air low-pressure flame. The instrument was checked by observation of combustion water-vapor lines, but it can be used for any molecules when the optical frequency of the semiconductor laser is changed.

2. Theory

A. Principle

The basic feature of heterodyne detection consists of the superimposing of two electric fields on a square-law photomixer: A radiation comes from the source to characterize, and a radiation comes from a reference laser called the local oscillator (LO). Let us consider a plane wave as the LO and a quasimonochromatic wave as the source.

When the second-order terms (self-beat of two spectral components of the source) are neglected, the photocurrent is given by

$$I_{ph}(t) = \frac{\eta e}{h\bar{\nu}} \left\{ \frac{P_{LO} + P_s}{2} + \int E_{LO} E_s(\omega) \times \cos[(\omega_{LO} - \omega)t - \varphi] d\omega \right\}, \quad (1)$$

where P_{LO} and P_s , respectively, are the LO and the source power, η is the effective heterodyne efficiency, and $\bar{\nu}$ is the mean optical frequency. Equation (1) indicates that the source spectral information is contained in the photocurrent but converted down into intermediate frequencies.

B. Photocurrent Analysis

So, the intermediate-frequency component of the photocurrent contains the source spectral information. More detailed theoretical developments of photomixing can be found in the literature.¹⁸⁻²⁰ In any case, the photocurrent analysis must be made at the photomixer output to extract the information of interest about the source.

Conventional techniques, based on fixed-frequency LO, consist of analyzing the photocurrent with complex devices such as filter banks,²¹ acousto-optical spectrometers,⁵ or superheterodyne rf mixing techniques.²² In these cases the setup rapidly becomes heavy and expensive; a high-speed photomixer is necessary, and the well-known problem of folding effect, owing to a double-side band detection, has to be taken into account.²³

In this paper we took advantage of the diode laser tunability. Indeed, if the LO is continuously tun-

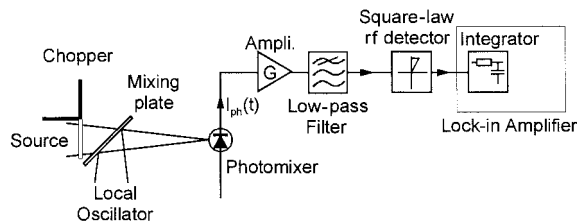


Fig. 1. Basic diagram of a tunable LO heterodyne radiometer. The signal-processing line is simple thanks to the LO continuous tunability. In the case of a fixed LO, a high-speed photomixer and a rf spectrometer (filter bank, acousto-optical spectrometer, or superheterodyne spectromete) would be required.

able, a simple rf low-pass filter or a low-bandwidth photomixer is convenient; see Fig. 1.

The low-pass filter fixes the half-analysis bandwidth of the system and therefore its resolution. The square-law rf detector delivers a voltage proportional to the rf power contained in the analysis bandwidth. As a consequence, the signal V_{het} at the radiometer output is directly proportional to the optical power integrated in the analysis bandwidth and centered on the LO frequency:

$$V_{het} \propto \int_{\omega_{LO} - (B/2)}^{\omega_{LO} + (B/2)} |E_s(\omega)|^2 d\omega. \quad (2)$$

By continuously adjustment of the LO frequency, the radiometer then records the part of the source spectrum in the LO tunability range.

C. Signal-to-Noise Ratio Considerations

In the ideal case, a heterodyne detector is shot noise limited. In this case, the postdetection signal-to-noise ratio (SNR) is²⁴

$$SNR = \frac{\eta P_s}{h\bar{\nu}B} \sqrt{B\tau}. \quad (3)$$

$\sqrt{B\tau}$ is the postdetection term of the radiometer (in the case of a Dicke radiometer), where B is the analysis bandwidth and τ is the integration time. This postdetection SNR expression is valid only if the power SNR is much smaller than unity. It is always the case for a radiometer detecting weak radiations. An explanation of the postdetection term's origin was given by Menzies.²⁵

In the term η , called the effective heterodyne efficiency, we include all the degradation parameters that can occur: beam misalignments,²⁶ photomixer quantum efficiency, transmitting optics and medium, amplitude modulation, and polarization sensitivity. In the case of radiometry, if gas emission linewidths are greater than B , as we will see in Section 4, the power emitted by the source can be expressed by

$$P_s = \lambda^2 B \epsilon(\nu) L_\nu^0(T), \quad (4)$$

where $\epsilon(\lambda)$ is the source emissivity factor, T is the source temperature, and L_ν^0 is the Planck radiance.

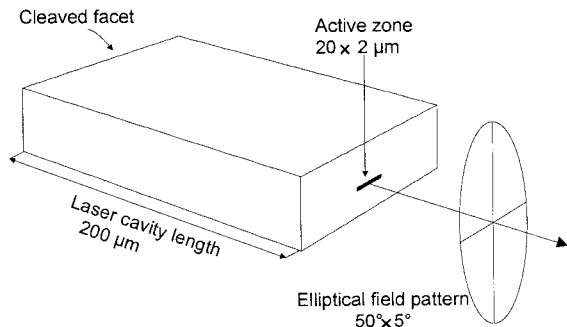


Fig. 2. Lead-salt laser with the typical geometric parameters. The emitted beam is elliptic and astigmatic.

As P_s is proportional to B , the SNR is directly proportional to $\sqrt{B\tau}$.

In the special case in which the LO is a semiconductor laser, some new noise features must be taken into consideration. Indeed, such a laser can produce excess noise owing to the multimode nature of its emission. The sensitivity of the heterodyne instrument is thus decreased. Harward and Sidney gave an analysis of the different kinds of excess noise from observed diode laser noise spectra.²⁷

In addition, the optical power emitted by mid-infrared diode lasers is often low. We can no longer keep the shot-noise-limited assumption. Menzies discussed the additional noise sources and their impact on the quality of a heterodyne radiometer.²⁵ Allario *et al.* proposed criteria for good operation with diode lasers used as LOs²⁸: 700 μW of power at the facet output, 80% of spectral purity, and an excess-noise-equivalent power less than 0.8 times the incident power on the photomixer. These criteria are extremely restrictive. A commercial laser that obeys all these criteria at one time is rare, and we have never worked under these diode laser operating conditions.

3. Instrumentation

A. Lead-Salt Lasers as Local Oscillators

In our experiment, a diode laser provided by Laser Components (Germany) was used as the LO. This component consists of a double heterojunction of lead-salt semiconductors working above the temperature of liquid nitrogen (80–110-K range). This laser has a Fabry–Perot cavity simply obtained by one cleaving the output facets. A sketch of the laser is given in Fig. 2.

Frequency tuning can be done either by varying the temperature or by varying the injection current. We explored and discussed these tuning mechanisms in a previous paper.²⁹ At best, the single-mode spectral range of continuous tuning that can be reached is 1.5 to 2 cm^{-1} with tuning rates of 19.6 cm^{-1}/A and 0.66 cm^{-1}/K . In this paper, once a convenient operating point was found, we kept the temperature fixed and applied an injection current ramp to tune the laser frequency.

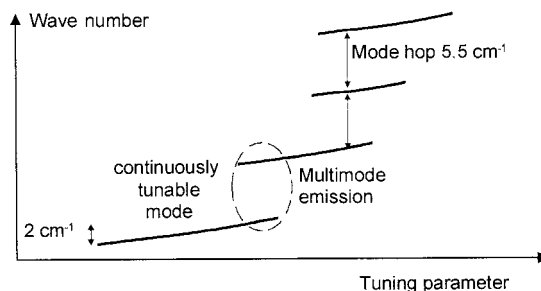


Fig. 3. Main spectral characteristics of a lead-salt laser. The continuously tunable spectral range is, at best, 2 cm^{-1} . The mode-hop spread depends on the laser cavity length and is in our case 5.5 cm^{-1} . At mode hops, a multimode emission often occurs.

The transition between two successive continuously tunable spectral zones is abrupt; it consists of a laser mode hop. The hop spread is directly defined by the laser cavity length and is, in our case, around 5.5 cm^{-1} . Between two single-mode zones, the laser often operates multimode. A LO multimode operation is not relevant for heterodyne detection: The partition noise would be prevalent, and any mode selection technique is useless.³⁰ Figure 3 shows a diagram of a lead-salt laser's spectral behavior. Clearly, to achieve heterodyne detection, one must know single-mode emission operating points. A complete laser-mode cartography is necessary.

The laser we used can cover a spectral range between 1315 and 1368 cm^{-1} with an almost good spectral quality (side-mode rejection > 1000) but a low output power (around 200 μW). Owing to the 5.5- cm^{-1} mode-hopping phenomenon, this covered range is, of course, discrete. To discriminate between low- and high-quality spectral modes, we inserted a high-finesse (approximately 30) confocal Fabry–Perot etalon in the laser optical path. It provides a 0.01- cm^{-1} relative frequency calibration. Figure 4 presents etalon signals when the laser emission reveals single and multimode emissions. The absolute frequency calibration of the laser was made via direct absorption spectroscopy through a reference gas cell.

This kind of laser has low spectral quality, typi-

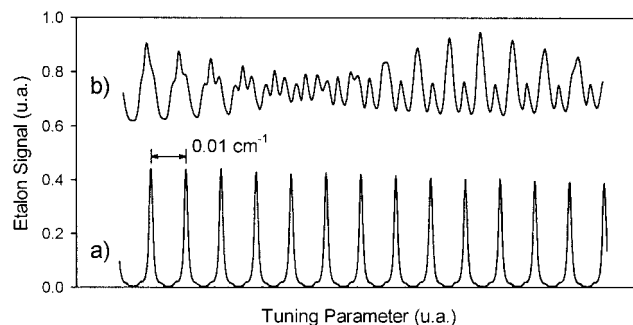


Fig. 4. Signals provided by the confocal Fabry–Perot etalon. From these records, a relative frequency calibration of the laser emission can be reached. In addition, they allow an optical diagnostic of the laser emission by discrimination of [trace (a)] single and [trace (b)] multimode emissions.

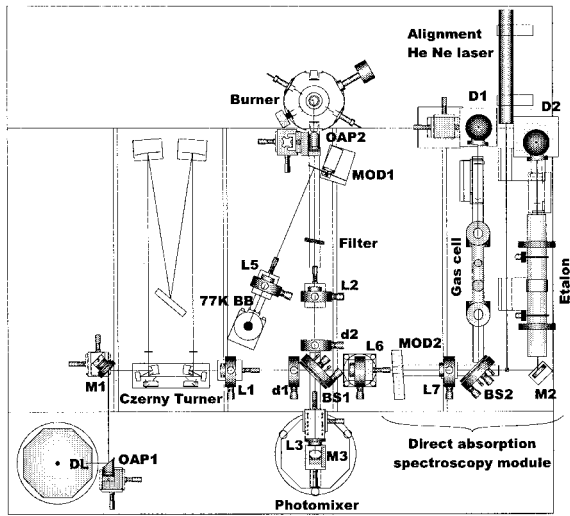


Fig. 5. Instrument-scaled optical setup.

cally, a longitudinal-mode spectral linewidth is between 10 and 100 MHz,^{31,32} and has low power compared with a gas laser. They are extremely sensitive to optical feedback. But these drawbacks are balanced by the continuous frequency tuning advantage. More details about these lasers can be found in the literature.³³

B. Burner as Optical Source

Our aim is to validate the efficiency of a heterodyne radiometer by probing the exhaust gases of a combustion reaction and therefore by recording molecular emission spectra of the species located in a postflame region. A specific, laboratory-built burner was designed.³⁴

This burner is able to generate a stable, low-pressure, flat premixed flame from methane and air. The system is equipped with a depression manometer and precision flow meters to control the methane–air mixture. The working pressure range is between 70 Torr and the atmospheric pressure. The reaction combustion mainly produces water and carbon dioxide. Here we are interested in detecting water vapor. The temperature in the postflame region is high owing to the exothermic reaction; water vapor then thermally emits radiation that goes through a BaF₂ window to be collected.

This radiation is combined with the lead-salt diode laser beam on the photomixer for heterodyne detection. The emission spectra will provide useful information on the abundance, the pressure, and the temperature of the probed species.

C. Instrument Design

The actual design of our heterodyne radiometer is given in Fig. 5. It is a scaled top view of the optical bench. Figure 6 is a simplified diagram of the optical arrangement.

The LO beam, emitted by the (diode laser) DL, is collected by a $f/2$ off-axis parabolic mirror (OAP1). It can go, or not, according to the flip mirror's posi-

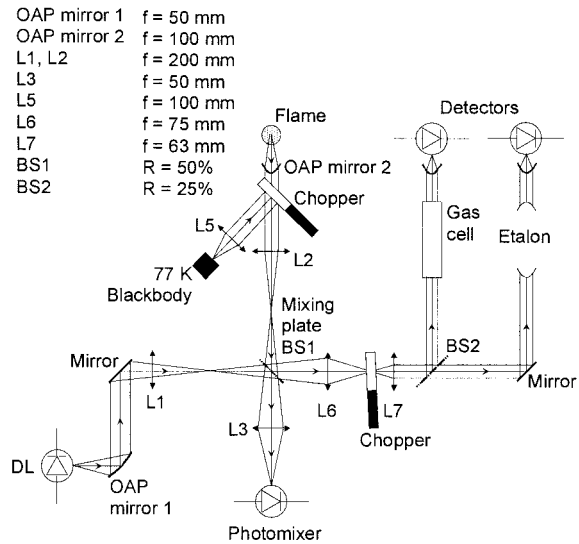


Fig. 6. Simplified optical diagram of the optical arrangement.

tion, through a Czerny–Turner spectrometer for coarse wavelength evaluation. An intermediate DL image is formed on the diaphragm d1 by the L1 lens. Then the LO beam is split into two parts by a ZnSe 50–50 beam splitter (BS1). The reflected beam is focused on the liquid-nitrogen-cooled HgCdTe photomixer, and the transmitted beam goes into the direct absorption spectroscopy module, which will be described later.

The signal beam, coming from the postflame region inside the burner, is collected by a $f/4$ off-axis parabolic mirror (OAP2) placed on an adjustable beam-steering mount. This signal can be chopped (MOD1) against a reference beam that comes from a 77-K blackbody in order to increase the thermal contrast.³⁵ A filter (low pass with a cutoff frequency of 1500 cm⁻¹) is placed in the source optical path to limit the optical bandwidth of intense sources. It is particularly useful when we use a 1500-K blackbody source instead of the burner for instrument alignment. An L2 lens forms an intermediate image of the source in the diaphragm d2, which is conjugated with d1 by BS1. The signal beam is then focused on the photomixer.

Now let us describe the direct absorption spectroscopy module used for diode laser frequency calibration. At the output of BS1, the L6 lens forms a DL image where the transmitted laser beam is chopped (MOD2). The beam is collected again by the L7 lens. Next, the beam is once again divided into two parts. The first one goes through a 20-cm reference gas cell, filled with 1 Torr of sulfur dioxide, for an absolute laser frequency calibration, and the other one goes through a confocal Fabry–Perot etalon for a relative frequency calibration and a laser spectral quality diagnostic.

As shown in Fig. 1, the photocurrent intermediate-frequency component is amplified by two 30-dB gain voltage amplifiers. A 90-MHz low-pass filter then defines the 180-MHz detection bandwidth of the in-

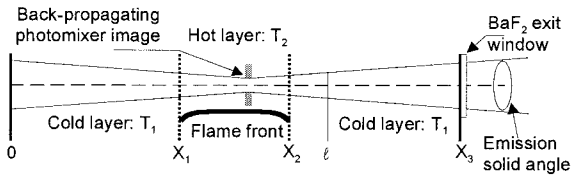


Fig. 7. Geometry used for the description of total flux emitted by molecules in the burner postflame region.

strument, namely, a 0.006-cm^{-1} resolution. The intermediate-frequency power is detected by a square-law rf diode, and the output signal is sent to a lock-in amplifier. The signal is numerically recorded by the acquisition system and saved on a computer hard drive.

4. Emission Basic Model

Before presenting the typical results, we are going to introduce an emission model describing the observed spectra.

We have to solve the radiative transfer equation under assumptions of local thermodynamic equilibrium and nonscattering medium. The one-dimensional general solution is given by

$$L_\nu(l) = L_\nu(0)\exp[-K(\lambda)l] + K(\lambda) \times \int_0^l L_\nu^0[T(x)]\exp[-K(\lambda)(l-x)]dx, \quad (5)$$

where $L_\nu(l)$ is the radiance at the l abscissa expressed in $\text{W m}^{-2} \text{Sr}^{-1} \text{Hz}^{-1}$, $K(\lambda)$ is the absorption coefficient, and T is the temperature. The total spectral optical power is

$$\Phi_\nu = \int_S \int_\Omega L_\nu(X_3)\cos(\theta)dSd\Omega, \quad (6)$$

where X_3 is the burner length as shown in Fig. 7, the integration is performed on the source surface S , and Ω is the emission solid angle. For the case of the heterodyne detection, the antenna theorem gives us a new constraint on the etendue, which is limited to the square of the wavelength.³⁶ With the small-angle approximation, the total detected flux in the instrument bandwidth B is then

$$\Phi = \lambda^2 \int_{\nu_{LO}-(B/2)}^{\nu_{LO}+(B/2)} L_\nu(X_3)d\nu \approx \lambda^2 B L_\nu(X_3), \quad (7)$$

with the realistic approximation that the detection bandwidth is small compared with the emission linewidth. Here B is 180 MHz.

Now we apply these notions to the burner's specific geometry sketched in Fig. 7. For modelization, the burner is divided into three isothermal layers with a mean effective temperature. This model was validated by previous absorption spectroscopy experiments.³⁴ There are two identical cold layers corresponding to the medium around the flame and a

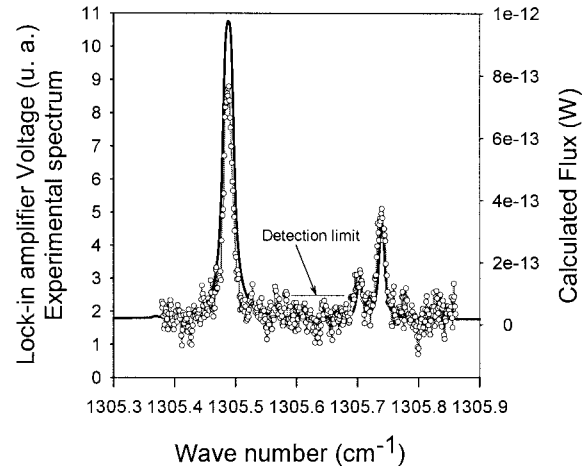


Fig. 8. Experimental and calculated spectra of combustion water vapor in the postflame region of the burner.

high-temperature layer corresponding to the postflame region.

Knowledge of $K(\lambda)$ is necessary for computing the resultant power, independently of the geometry. This quantity depends on temperature, so we calculate it by using the spectroscopic HITEMP96 database, the high-temperature extension of HITRAN96.³⁷ $K(\lambda)$ is pressure dependent, too, and we assume that pressure is identical in the three layers.

5. Typical Spectrum

Figure 8 is a plot of an experimental spectrum and the corresponding calculated one (solid curve).

The flame used is a 93-Torr one. Methane and air are injected, respectively, at flows of 0.4 and 2.2 g/min. To record this spectrum, we tuned the diode laser with a 28-mA spread current ramp around 1020 mA. The diode laser's temperature is fixed at 96 K. The analysis bandwidth is 180 MHz. The integration time is 1 s, and the acquisition time is 2 s. So the total spectrum recording time is 17 min. In regard to the LO, it generates a 130- μA photocurrent. This corresponds to an incident power on the photomixer of, at best, 100 μW .

On this water-vapor emission spectra, a line from the ν_2 vibrational band and two lines from the $2\nu_2-\nu_2$ hot band appeared, whose spectroscopic data, taken from Hitemp96, are listed in the Table 1.

The parameters used for the calculated spectrum are as follows: a temperature of 2200 K for the high-temperature layer, which is the theoretical CH_4 -air

Table 1. HITEMP96 Data for 2000-K Lines Observed on the Experimental Spectrum

Frequency (cm^{-1})	Line Strength ($\text{cm}^{-1}/\text{molecule cm}^{-2}$)	Lower State Energy (cm^{-1})	Vibrational Band
1305.488100	2.193×10^{20}	2225.4690	ν_2
1305.703061	2.298×10^{21}	3391.1310	$2\nu_2-\nu_2$
1305.739657	6.911×10^{21}	3391.1260	$2\nu_2-\nu_2$

Table 2. Experimental Parameters Used in the Emission Model to Compute the Calculated Spectra of Fig. 8

Parameters	Values
Cold-layer temperature	800 K
Hot-layer temperature	2200 K
Partial water-vapor pressure	28.6 Torr
Air-broadening pressure	65 Torr
Radiometer analysis bandwidth	180 MHz
Background radiance	L_v^0 (300 K)
Hot-layer length	25 mm
Cold-layer length	34.5 mm

combustion temperature, and an effective temperature of 800 K for the cold layer. This temperature was fitted to take into account temperature and concentration profiles in the burner. The flow-meter's measurements give us a water-vapor pressure of 28.6 Torr and an air-broadening pressure of 65 Torr. The analysis bandwidth is 180 MHz, and the radiance at the abscissa origin is the one of a 300-K blackbody. The burner length is 94 mm, and the hot-layer length corresponds to the flame diameter: 25 mm. All the parameters used in our emission model to compute the calculated spectra are listed in Table 2.

The first calculated line on the left is overestimated. Indeed, the calculated flux is the one at the output of the burner. We did not take into account the atmospheric water-vapor absorption occurring on the LO and source optical legs for this frequency, which is of the order $1.7 \times 10^{-2} \text{ m}^{-1}$. In any case, here our aim is to perform a first validation. To reach retrieved quantitative information, such as concentration or temperature profiles, one must develop a sophisticated algorithm.

For the doublet on the right, atmospheric vapor does not interfere: At these frequencies the atmospheric absorption coefficient is around 4×10^{-5} and $9 \times 10^{-5} \text{ m}^{-1}$.

Under our experimental conditions, as we can see, the left line of the doublet is nearly at the detection limit of the instrument. From the inspection of the experimental spectra, we deduced the noise level and a detection limit of $1.3 \times 10^{-13} \text{ W}$ (equivalent blackbody temperature of 450 K) with a 100- μW LO power. The theoretical detection limit of a perfect heterodyne receiver would be $7 \times 10^{-16} \text{ W}$ (equivalent blackbody temperature of 200 K).

6. Concluding Remarks

This paper has shown that a tunable diode laser heterodyne radiometer is actually relevant for combustion-process remote measurements. Here we have designed an instrument using a lead-salt diode laser as a tunable local oscillator. We used it to detect water-vapor emission spectra in the burned gas region of a methane-air premixed flat flame. For this purpose we have presented a spectrum recorded in the spectral region of 1315 cm^{-1} . Our instrument has been proven to be able to passively

detect fluxes of the order of $1.3 \times 10^{-13} \text{ W}$ with a 0.006-cm^{-1} resolution.

First, we undertook this paper to validate the use of a tunable laser heterodyne radiometer for combustion detection and diagnostic. As infrared molecular spectra represent a perfect signature of molecules, such an instrument could be useful as qualitative remote detector of any high-temperature gas. Such an instrument can be applied to characterize combustion in an aircraft thrust nozzle or any engine jet pipe. Detecting high-temperature pollutants involved in industrial plants that use burners could be a useful application, too.

A future direction will be to work on quantitative inversion models. Quantitative measurements become relevant when some information about the source can be reached.⁷ If the temperature profile of the probed source is known, the concentration profile can be retrieved and, vice versa. For example, the instrument can be relevant for remote pollutant-concentration measurements in any exhaust duct. In the case of an isothermal medium, the two-line method can provide temperature, and, from emission line shape, concentration can thus be deduced.

The heterodyne detection is particularly attractive for remote and passive characterization of distant sources owing to its etendue limitation. This characteristic can be useful for concentration or temperature cartography or both.

The first and main way to improve the heterodyne radiometer detection limit is to use a more suitable LO. The quantum cascade lasers³⁸ are promising as heterodyne system LO.³⁹ Compared with lead-salt lasers, their tunability is reduced, but the power emitted is of several milliwatts, and the spectral quality is better.

In this paper we used a laboratory burner as the source. For real combustion processes, such as industrial burners or aircraft thrust nozzles, the flux emitted will be greater because combustion temperature will be higher.

The authors greatly thank R. T. Menzies of the Jet Propulsion Laboratory for supplying interesting remarks and useful advice about this paper.

References

1. R. T. Menzies and M. S. Shumate, "Air pollution: remote detection of several pollutant gases with a laser heterodyne radiometer," *Science* **184**, 570–571 (1974).
2. S. R. King, D. T. Hodges, T. S. Hartwick, and D. H. Barker, "High resolution atmospheric transmission measurement using a laser heterodyne radiometer," *Appl. Opt.* **12**, 1106–1107 (1973).
3. R. K. Seals and B. J. Peyton, "Remote sensing of atmospheric pollutant gases using an infrared heterodyne spectrometer," *Ann. IEEE* **10-5**, 1–6 (1976).
4. C. Thiebaux, D. Courtois, A. Delahaigue, H. Le Corre, J. C. Mouanda, and A. Fayt, "Dual beam laser heterodyne spectrometer: ethylene absorption spectrum in the 10 μm range," *Appl. Phys. B* **47**, 313–318 (1988).
5. S. L. Jain, "Laser heterodyne system for measurement of minor constituents in the atmosphere," *Indian J. Radio Space Phys.* **25**, 309–317 (1996).

6. R. T. Menzies, "Remote detection of SO₂ and CO₂ with a heterodyne radiometer," *Appl. Phys. Lett.* **22**, 592–593 (1973).
7. T. Kostiuik and M. J. Mumma, "Remote sensing by IR heterodyne spectroscopy," *Appl. Opt.* **22**, 2644–2654 (1983).
8. A. L. Betz, M. A. Johnson, R. A. McLaren, and E. C. Sutton, "Heterodyne detection of CO₂ emission lines and wind velocities in the atmosphere of Venus," *Astrophys. J.* **208**, L141–L144 (1976).
9. J. H. McElroy, "Infrared heterodyne solar radiometry," *Appl. Opt.* **11**, 1619–1622 (1972).
10. Y. Shani, A. Hardy, E. Kapon, and A. Katzir, "The far field of PbSnTe injection lasers," *IEEE J. Quantum Electron.* **QE20**, 1297–1269 (1984).
11. M. Agne, A. Lambrecht, U. Schiessl, and M. Tacke, "Guided modes and far field patterns of lead chalcogenide buried heterostructure laser diodes," *Infrared Phys. Technol.* **35**, 47–58 (1994).
12. M. A. Frerking and D. J. Muehlner, "Infrared heterodyne spectroscopy of atmospheric ozone," *Appl. Opt.* **16**, 526–528 (1977).
13. J. M. Hoell, C. N. Harward, and W. Lo, "High resolution atmospheric spectroscopy using a diode laser spectrometer," *Opt. Eng.* **21**, 320–326 (1982).
14. D. Glenar, T. Kostiuik, D. E. Jennings, D. Buhl, and M. J. Mumma, "Tunable diode laser heterodyne spectrometer for remote observation near 8 μm ," *Appl. Opt.* **21**, 253–259 (1982).
15. H. Fukunishi, S. Okano, M. Taguchi, and T. Ohnuma, "Laser heterodyne spectrometer using a liquid nitrogen cooled tunable diode laser for remote measurements of atmospheric O₃ and N₂O," *Appl. Opt.* **29**, 2722–2728 (1990).
16. B. Parvitte, C. Thiébaux, and D. Courtois, "Tunable heterodyne spectrometer in the 9 μm range with selected lead salt diodes," *Spectrochim. Acta Part A* **55A**, 2027–2037 (1999).
17. F. Schmülling, B. Klumb, M. Harter, R. Schieder, B. Vowinkel, and G. Winnewisser, "High-sensitivity mid-infrared heterodyne spectrometer with a tunable diode laser as a local oscillator," *Appl. Opt.* **37**, 5771–5776 (1998).
18. O. Andrade and B. J. Rye, "Tolerances in optical mixing," *J. Physics D* **7**, 280–291 (1974).
19. H. Z. Cummins and H. L. Swinney, "Light beating spectroscopy," in *Progress in Optics*, E. Wolf, ed. (North-Holland, Amsterdam, 1970), Vol. 8.
20. L. Mandel, "Heterodyne detection of weak light beam," *J. Opt. Soc. Am.* **56**, 1200–1206 (1966).
21. M. J. Mumma, T. Kostiuik, D. Buhl, G. Chin, and D. Zipoy, "Infrared heterodyne spectroscopy," *Opt. Eng.* **21**, 313–319 (1982).
22. D. Courtois, C. Thiébaux, and A. Delahaigue, "Heterodyne spectrometer for the 10 μm region," *Int. J. Infrared Millim. Waves* **5**, 185–195 (1984).
23. C. Thiébaux, A. Delahaigue, D. Courtois, and J. C. Mouanda, "Heterodyne spectra analysis," *Int. J. Infrared Millim. Waves* **12**, 759–767 (1992).
24. T. G. Blaney, "Signal-to-noise ratio and other characteristics of heterodyne radiation receivers," *Space Sci. Rev.* **17**, 691–702 (1975).
25. R. T. Menzies, "Laser heterodyne detection techniques," in *Laser Monitoring of the Atmosphere*, E. D. Hinkley, ed. (Springer-Verlag, Berlin, 1976), Chap. 7.
26. S. C. Cohen, "Heterodyne detection: phase front alignment, beam spot size, and detector uniformity," *Appl. Opt.* **14**, 1953–1959 (1975).
27. C. N. Harward and B. D. Sidney, "Excess noise in Pb_{1-x}Sn_xSe semiconductor lasers," in *Proceedings of an International Conference on Heterodyne Systems and Technology*, NASA Conference Publication 2138 (NASA, Williamsburg, Va., 1980), pp. 129–142.
28. F. Allario, S. J. Katzberg, and J. C. Larsen, "Sensitivity studies and laboratory measurements for the laser heterodyne spectrometer experiment," in *Proceedings of an International Conference on Heterodyne Systems and Technology*, NASA Conference Publication 2138 (NASA, Williamsburg, Va., 1980), pp. 221–240.
29. D. Weidmann and D. Courtois, "High quality infrared (8 μm) diode laser source design for high resolution spectroscopy with precise temperature and current control," *Infrared Phys. Technol.* **41**, 361–371 (2000).
30. K. Peterman, *Laser Diode Modulation and Noise* (Kluwer Academic, London, 1991).
31. J. Reid, D. T. Cassidy, and R. T. Menzies, "Linewidth measurements of tunable diode lasers using heterodyne and etalon techniques," *Appl. Opt.* **21**, 3961–3965 (1982).
32. R. Brunner and M. Tacke, "Tunable diode laser line width and tuning measurements for gas analysis monitoring," *Infrared Phys. Technol.* **43**, 61–67 (2002).
33. G. P. Agrawal and N. K. Dutta, *Long Wavelength Semiconductor Lasers* (Van Nostrand Reinhold, New York, 1986).
34. D. Weidmann, A. Hamdouni, and D. Courtois, "CH₄/air/SO₂ premixed flame spectroscopy with a 7.5 μm diode laser," *Appl. Phys. B* **73**, 85–91 (2001).
35. D. Courtois, A. Delahaigue, and C. Thiébaux, "Detection of thermal emission from atmospheric gases by laser heterodyne radiometry," *Infrared Phys.* **34**, 407–413 (1993).
36. A. E. Siegman, "The antenna properties of optical heterodyne receivers," *Proc. IEEE* **54**, 1350–1356 (1966).
37. L. S. Rothman, C. P. Rinsland, A. Goldman, S. T. Massie, D. P. Edwards, J. M. Flaud, A. Perrin, C. Camy-Peyret, V. Dana, J. Y. Mandin, J. Schroeder, A. McCann, R. R. Gamache, R. B. Wattson, K. Yoshino, K. V. Chance, K. W. Jucks, L. R. Brown, V. Nemtchinov, and P. Varanasi, "The HITRAN molecular spectroscopic database and HAWKS (HITRAN Atmospheric Workstation): 1996 edition," *J. Quant. Spectrosc. Radiat. Transfer* **60**, 665–710 (1998).
38. J. Faist, A. Tredicucci, F. Capasso, C. Sirtori, D. L. Sivco, J. N. Baillargeon, A. L. Hutchinson, and A. Y. Cho, "High-power continuous-wave quantum cascade lasers," *IEEE J. Quantum Electron.* **34**, 336–343 (1998).
39. G. Sonnabend, D. Wirtz, and R. Schieder, "THIS-Infrared remote sensing with a tunable and transportable heterodyne spectrometer," paper B13 presented at the Third International Conference on Tunable Diode Laser Spectroscopy, Zermatt, Switzerland, July 8–12, 2001.